Published in final edited form as:
Angew Chem Int Ed Engl. 2012 July 23; 51(30): 7519–7522. doi:10.1002/anie.201201902.

Acoustic Droplet Vaporization and Propulsion of Perfluorocarbon-Loaded Microbullets for Targeted Tissue Penetration and Deformation

Daniel Kagan[†],
Department of Nanoengineering, University of California San Diego, 9500 Gilman Drive, La Jolla, CA 92093, USA

Michael J. Benchimol[†],
Department of Electrical and Computer Engineering, University of California San Diego, 9500 Gilman Drive, La Jolla, CA 92093, USA

Jonathan C. Claussen[†],
Department of Nanoengineering, University of California San Diego, 9500 Gilman Drive, La Jolla, CA 92093, USA

Erdembileg Chuluun-Erdene,
Department of Nanoengineering, University of California San Diego, 9500 Gilman Drive, La Jolla, CA 92093, USA

Sadik Esener, and
Department of Nanoengineering, University of California San Diego, 9500 Gilman Drive, La Jolla, CA 92093, USA

Joseph Wang
Department of Nanoengineering, University of California San Diego, 9500 Gilman Drive, La Jolla, CA 92093, USA

Sadik Esener: sesener@ucsd.edu; Joseph Wang: josephwang@ucsd.edu

Abstract

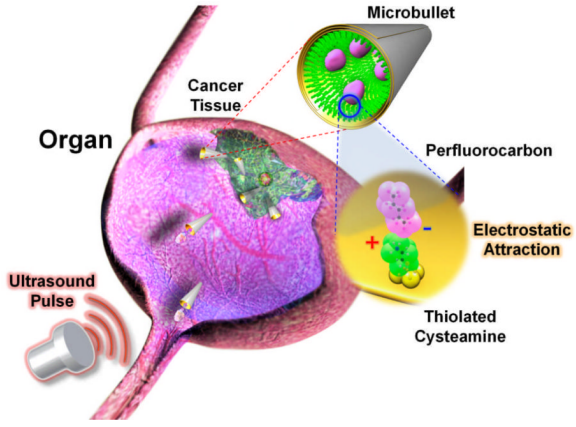

Correspondence to: Sadik Esener, sesener@ucsd.edu; Joseph Wang, josephwang@ucsd.edu.

[†]These authors contributed equally to this work.

Supporting information for this article is available on the WWW under http://www.angewandte.org or from the author.

Acoustic droplet vaporization of perfluorocarbon-loaded microbullets triggered by an ultrasound pulse provides the necessary force to penetrate, cleave, and deform cellular tissue for potential targeted drug delivery and precision nanosurgery.

Keywords

microrocket/microbullet; acoustic droplet vaporization; perfluorinated solvents; electrostatic interactions; tissue penetration

Recent advances in micro/nanomachines have shown great promise in diverse fields.[1–13] A wide variety of chemically-powered and magnetically-propelled micro/nanoscale machines have been developed for specific biomedical applications ranging from lab-on-chip bioanalytical devices to site-specific drug delivery targeting. However, these micro/nanomachines lack the power and biocompatibility necessary for penetrating tissue and cellular barriers, for *in vivo* cargo delivery and precision nanosurgery.

Prevalent micro/nanomachine designs typically require conversion of external chemical energy, harvested from the vicinity of the machines, to promote autonomous propulsion. Several mechanisms have been developed to realize such micro/nanomachine thrust in connection to hydrogen-peroxide fuel, including self-electrophoresis,[3,5] self-diffusiophoresis,[4] and bubble propulsion.[7,11,14] To enhance biocompatibility several groups have also explored fuel-free micro/nanomachine propulsion mechanisms, including the utilization of electrical power (i.e., diode nanowires)[15] and magnetic actuation.[16–18] Despite the inherent advantages of such externally-propelled micro/nanoscale locomotion schemes, these propulsion mechanisms do not possess the thrust needed for penetrating tissue barriers and cellular membranes.[19]

Herein we present a highly efficient microscale propulsion technique that utilizes ultrasound (US) to vaporize biocompatible fuel (i.e., perfluorocarbon PFC emulsions) bound within the interior of a micromachine for high velocity, bullet-like propulsion. Such remarkable micro/nanomachine thrust is sufficient for deep tissue penetration and deformation. An increase in enthalpy which accompanies vaporization results in energy transfer. Momentum, geometrically focused by virtue of the micromachine structure, generates projectile motion. Thus, instead of creating a medium which can convert a chemical fuel, we have produced a micromachine with an on-board fuel source capable of releasing energy independent of the surrounding environment via an external control.

Recently, gas and liquid PFC particles have received considerable attention due to their biocompatible nature for intravenous injection and subsequent destruction upon ultrasound irradiation.[20,21] The decreased solubility and low diffusion coefficient of these droplets and bubbles lengthens blood circulation before an incident US wave is used to induce their destruction or cavitation.[22] PFC microbubbles or emulsions are thus extremely attractive for diverse biomedical applications such as externally-triggered site-specific drug and gene delivery capsules[23–24], molecular imaging agents,[25] phase change contrast agents,[26,27] and blood substitutes.[27,29] However, we are unaware of earlier reports on using PFCs as an integrated fuel source for micro/nanomachine propulsion.

Similar to the externally triggered explosion experienced within a gun barrel to propel a bullet,[30] these micromachines, named here microbullets (MB), utilize for propulsion the rapid expansion and vaporization of perfluorocarbon droplets[31] electrostatically bound within the machine interior and triggered by an US pulse (i.e., acoustic droplet vaporization (ADV)).[32,33] These new US-triggered, PFC-loaded microbullets can travel at remarkably

high average velocities (~6.3 m s^{-1}: over 100 times faster than currently published micromachines)[11–14] and deeply penetrate and deform kidney tissue. The concomitance of powerful MB propulsion, biocompatible PFC emulsion fuel,[35] and deeply penetrative, yet medically safe US[34] could lead to highly targeted *in vivo* drug delivery, artery cleaning, gene regulation schemes, and cancer therapeutics that require higher specificity and accuracy than the current state-of-the-art.

The choice of the specific PFCs is also crucial as their chemical properties have profound effect upon the efficiency of the ADV process and hence upon the resulting propulsion performance. Low boiling point PFCs, such as perfluoropropane and perfluorobutane, are stable in the gaseous state, and have been extensively used for the production of microbubbles for contrast-enhanced US imaging.[41] Higher boiling point PFCs exist as liquids or solids, but two particular molecules, perfluoropentane (PFP) (TB = 29°C at 1 atm) and perfluorohexane (PFH) (TB = 56°C at 1 atm) are liquid PFCs which can also persist in the gaseous state—an important property for acoustic droplet vaporization (ADV). Thus, in this work, we distinctly functionalize micromachines with both PFH and PFP to optimize the US-triggered propulsion strategy.

A three-step fabrication strategy (Figure 1) was utilized for preparing the US-triggered MBs, including nanofabrication, cysteamine functionalization, and PFC emulsion binding. Large MBs (length ~40μm, Figure 1) were created via rolled-up thin-film nanofabrication techniques,[7, 11] while small MBs (length~8μm) utilized membrane-template electrodeposition for fabrication (see Experimental Methods in Supporting Information).[14] An embedded Ni layer facilitates MB magnetic washing and experimental alignment before US pulsing to facilitate directed, linear motion during propulsion. The inner Au layer of these microtubes permits cysteamine monolayer conjugation for electrostatic attachment of PFC droplets. The slightly tapered conical structure of the MBs, owing to the angled physical vapor deposition fabrication process,[7,11] directs thrust from ADV while an embedded magnetic layer permits externally-guided, magnetic alignment for precision steering.

To initiate this study, emulsion droplets of PFH (TB = 56 °C),[38] were utilized because they maintain stability under physiological conditions but enable ADV upon arrival of incident US pressure waves. In addition, the emulsion composition was designed to have efficient matching of intermolecular forces between the PFC and the surfactant, necessary to reduce interfacial tension and facilitate the conversion of nanoscale droplets. To illustrate the selective PFH droplet immobilization strategy developed herein, fluorescently-tagged PFH emulsions, stabilized by a negatively-charged surfactant, were electrostatically immobilized onto the cysteamine-modified inner gold surfaces (Figure SI 1). The exposed amine group (pKa 8.6) of the cysteamine[39] is positively charged for the prescribed experimental settings (i.e., pH range 7.4 - 8.0) and thus electrostatically binds to emulsions stabilized with an anionic phosphate fluorosurfactant (pKa 7.2). Emulsions were strongly negative with a measured zeta potential of −46 mV in phosphate buffered saline. Graphical representation of the emulsion size distribution (mean = 304.9 nm, PDI = 0.144) and stability is included in the Supporting Information.

Initial US-triggered propulsion experiments reveal PFH emulsion vaporization originating from within the MBs (Figure 2a and Video SI 1). A vaporized emulsion (i.e., bubble) extending out of the tail of the MB is clearly visible after the US pulsation (Figure 2a, right), corroborating the assumption that microscale gaseous bubble formation is resultant upon sudden US-triggered, PFH droplet vaporization. The rapid emulsion expansion during the vaporization process (~5 fold radial)[21] provides a sudden impulse that projects the MB out of the microscope field of view within an extremely short single image frame (~55.6 μs).

Control experiments over a longer period demonstrate that nonspecific adsorption of PFH was negligible as MBs functionalized without cysteamine (Figure 2c) or without the PFH emulsion (Supporting Video 1) failed to produce bubbles nor MB movement. US pulsations therefore have minimal effect on the locomotion of non-functionalized MBs.

The movement of the MBs were analyzed over a series of frames (Figure 2b obtained from Video SI 2) in which the MB travels 350 μm from its initial location within 55.6 μs upon vaporization of the PFH emulsion [Figure 2b (left), dotted circle] triggered by an US pulse signal. Therefore, the MB traveled at a remarkably high average velocity of 6.3 m s^{-1}, which corresponds to an ultrafast relative velocity of over 158,000 body-length s^{-1}. The MB dynamics were analyzed with Stokes' Law and experimental image analysis (see Supporting Information). The initial MB velocity (56.9 s^{-1}), kinetic energy (0.764 nJ) and momentum (2.69e-11) were calculated with Eqs. (1–3) in conjunction with MB parameter values presented in Table SI 1 (see Supporting Information for equation derivations and parameter values):

$$\upsilon_0 = \frac{\Delta d}{\frac{m}{k}\left(1 - \frac{m}{k}e^{-\frac{k\Delta t}{m}}\right)} \quad (1)$$

$$E_k = \frac{1}{2}m\upsilon^2 \quad (2)$$

$$p_0 = m\upsilon_0 \quad (3)$$

where k is the drag coefficient for a cylinder, m is the mass of the hollow MB (kg), Δd is distance traveled (m), t is time (s), and E_k is kinetic energy (J). The remarkably high initial and average MB velocities associated with US-triggered emulsion vaporization compare favorably with velocities achieved for stochastically moving microparticles propelled by water cavitation.[40]

In order to promote highly efficient, single-shot, and controllable MB firings, the US trigger settings (i.e., transducer pressure and pulse length) and MB fabrication (i.e., size, shape, thickness) were optimized at distinct settings. The combination of low pressure (1.6 MPa)/ medium pulse length (44 μs) and high pressure (3.8 MPa)/short pulse length (4.4 μs) produced efficient linear MB locomotion from ADV without external water cavitation, while other combinatoral changes in pulse pressure and length produced water cavitation and/or sporadic MB movement (see Figure SI 2, 5, and 6). Furthermore distinctly sized MBs (40 nm thick, 40 μm long and 2.5 μm in diameter) produced ultrafast linear motion when functionalized with 180 nm diameter-sized PFH emulsions. However, MBs that were longer (lengths > 100 μm), longer and slender (60 μm long, 400 nm thick, 3 μm in diameter), and smaller MBs (8 μm long, 800 nm inner diameter) rotated uncontrollably (Figure SI 3 and Video SI 3), exploded (Figure SI 4 and Video SI 4), and stochastically agitated (Video SI 5) upon US pulse firing. Additional functionalization tests, revealed that lower boiling point emulsions (pPFP, BP: 30 °C)[38] vaporized more consistently at low pressures but were less stable during functionalization and increased MB explosion during US triggering. Further optimization of the emulsion size and composition could thus be used to tailor US triggered propulsion devices for specific biomedical applications that require distinct microbullet velocity and momentum characteristics.

To demonstrate the ability to penetrate through dense materials for potential targeted delivery applications, PFH-loaded MBs were fired into tissue sections from a lamb kidney.

The image sequence (Figure 3a) and Video SI 6 depict the deep penetration of the MB into the lamb kidney tissue section after an US pulse. These sequential images illustrate the MB before locomotion, during initial tissue penetration, and after traveling 200 μm into the tissue from a single 44 μsec, 1.6 MPa US pulse. A very short US pulse (4.4 μsec) at high pressure (3.8 MPa) also provided sufficient thrust for the MBs to pierce kidney tissue (Figure SI 5 and SI Video 7). Video SI 8 and Figure 3b depict the ability of the US-triggered MB to penetrate, deform, and cleave kidney tissue. Progressive images illustrate the MB capturing, deforming, and transporting a small piece of kidney tissue after a 44 μsec, 1.6 MPa US pulse (Figure 3b). Thus, the US pulse pressure can be tuned to permit MB tissue piercing, deformation, or deep penetration, depending upon the specifications and tissue degradation restrictions of distinct biomedical applications. Furthermore, the ability to propel multiple MBs from the same US pulse into a tissue section is displayed in Figure 3c and Video SI 9. The potential power of multiple US-triggered MBs can be visualized as the MBs increase the tissue cavity area by 120% after the first 4.4 μsec/3.8 MPa US pulse and penetrate the kidney tissue after a second, similiarly tuned US pulse (see Figure SI 6 for full image sequence).

The presented ultrasound-triggered microbullet firing technique potentially offers a safe, low-cost, and effective method to project delivery devices into dense tissue or organs. These US-triggered, PFC-loaded MBs possess the unique ability to accelerate rapidly, acquire significant momentum (2.69×10^{-11} Ns), and travel at average speeds over 6 m s^{-1} (i.e., approximately 100 times faster than previous micromachines). This unprecedented MB speed and force enables lamb kidney tissue piercing, deep penetration, deformation, and cleaving—capabilities that, to our knowledge, have never been demonstrated with micro/nanomachines. The US-triggered MB propulsion technique is highly reproducible, with approximately 80% of perfluorohexane conjugated microbullets fire upon US pulsing, and MBs display negligible damage after multiple firing under optimized US conditions. The larger 40μm microrockets were generally used in this study for visualization purposes, but the use of smaller 8 μm microbullets suggest that this is a scalable approach, opening the door for potential use in capillaries that are 5 – 10 μm in diameter. This US-triggered MB propulsion strategy should thus have a tremendous impact on diverse biomedical applications (e.g., targeted drug delivery, circulating biolistics, micro-tissue and artery-cleaning/removal schemes, precision nanosurgery, and cancer therapeutics). For example, as an alternative to Bacillus Calmette-Guerin (BCG) treatment for bladder cancer as illustrated in Figure 3c, multiple US-triggered MBs could be introduced and fired into the bladder to create a natural inflammatory response for fighting cancer cells. While offering a similar immunoprophylactic effect, use of these MBs may potentially eliminate harmful side effects (e.g., sepsis, dysuria, hematuria, nausea, and fever) associated with BCG.

Supplementary Material

Refer to Web version on PubMed Central for supplementary material.

Acknowledgments

The authors gratefully acknowledge financial support from the National Science Foundation (Award Number CBET 0853375), National Cancer Institute (NCI-5U54CA119335-05), and the National Institutes of Health (NIH R25-CA153915). The authors thank Wei Gao for help in preparing the small MBs (length ~ 8 μm).

References

1. Mallouk T, Sen A. Sci. Am. 2009; 300:72. [PubMed: 19438052]
2. Ozin GA, Manners I, Fournier-Bidoz S, Arsenault A. Adv. Mater. 2005; 17:3011.
3. Pumera M. Nanoscale. 2010; 2:1643. [PubMed: 20680201]

4. Howse JR, Jones RAL, Ryan AJ, Gough T, Vafabakhsh R, Golestanian R. Phys. Rev. Lett. 2007; 99:48102.
5. Kline TR, Paxton WF, Mallouk TE, Sen A. Angew. Chem. Int. Ed. 2005; 44:744.
6. Wang J. ACS Nano. 2009; 3:4. [PubMed: 19206241]
7. Mei Y, Solovev AA, Sanchez S, Schmidt OG. Chem. Soc. Rev. 2011; 40:2109. [PubMed: 21340080]
8. Mirkovic T, Zacharia NS, Scholes GD, Ozin GA. Small. 2010; 6:159. [PubMed: 19911393]
9. Kagan D, Laocharoensuk R, Zimmerman M, Clawson C, Balasubramanian S, Bishop D, Sattayasamitsathit S, Zhang L, Wang J. Small. 2010; 6:2741. [PubMed: 20979242]
10. Sanchez S, Solovev AA, Harazim SM, Schmidt OG. J. Am. Chem. Soc. 2011; 133:701. [PubMed: 21166412]
11. Solovev AA, Mei Y, Bermudez Urena E, Huang G, Schmidt OG. Small. 2009; 5:1688. [PubMed: 19373828]
12. Balasubramanian S, Kagan D, Jack Hu CM, Campuzano S, Lobo-Castanon MJ, Lim N, Kang DY, Zimmerman M, Zhang L, Wang J. Angew. Chem. Int. Ed. 2011; 50:4161.
13. Huang G, Wang J, Mei Y. J. Mater. Chem. 2012; 22:6519.
14. Gao W, Sattayasamitsathit S, Orozco J, Wang J. J. Am. Chem. Soc. 2011; 133:11862. [PubMed: 21749138]
15. Calvo-Marzal P, Sattayasamitsathit S, Balasubramanian S, Windmiller JR, Dao C, Wang J. Chem. Comm. 2010; 46:1623. [PubMed: 20177595]
16. Gao W, Sattayasamitsathit S, Manesh KM, Weihs D, Wang J. J. Am. Chem. Soc. 2010; 132:14403. [PubMed: 20879711]
17. Ghosh A, Fischer P. Nano Lett. 2009; 9:2243. [PubMed: 19413293]
18. Zhang L, Abbott JJ, Dong L, Peyer KE, Kratochvil BE, Zhang H, Bergeles C, Nelson BJ. Nano Lett. 2009; 9:3663. [PubMed: 19824709]
19. Gao W, Kagan D, Pak OS, Clawson C, Campuzano S, Chuluun-Erdene E, Shipton E, Fullerton EE, Zhang L, Lauga E, Wang J. Small. 2011; 8:460. [PubMed: 22174121]
20. Bertilla SM, Thomas JL, Marie P, Krafft MP. Langmuir. 2004; 20:3920. [PubMed: 15969380]
21. Worah DM, Kessler DR, Meuter AR, Huang MG, Correas J-M, Quay SC. Drugs Future. 1997; 22:378.
22. Lentacker I, De Smedt SC, Sanders NN. Soft Matter. 2009; 5:2161.
23. Hernot S, Klibanov AL. Adv. Drug Deliver. Rev. 2008; 60:1153.
24. Unger EC, Porter T, Culp W, Labell R, Matsunaga T, Zutshi R. Adv. Drug Deliver. Rev. 2004; 56:1291.
25. Schutt EG, Klein DH, Mattrey RM, Riess JG. Angew. Chem. Int. Ed. 2003; 42:3218.
26. Reznik N, Williams R, Burns PN. Ultrasound Med. Biol. 2011; 37:1271. [PubMed: 21723449]
27. Sheeran PS, Luois SH, Mullin LB, Matsunaga TO, Dayton PA. Biomaterials. 2012; 33:3262. [PubMed: 22289265]
28. Riess JG. Chem. Rev. 2001; 101:2797. [PubMed: 11749396]
29. Biro GP, Blais P, Rosen AL. Crit. Rev. Oncol. Hematol. 1987; 6:311. [PubMed: 3549022]
30. Park HC, Byun KT, Kwak HY. Chem. Eng. Sci. 2005; 60:1809.
31. Wong ZZ, Kripfgans OD, Qamar A, Fowlkes JB, Bull JL. Soft Mater. 2011; 7:4009.
32. Kripfgans OD, Fowlkes JB, Miller DL, Eldevik OP, Carson PL. Ultrasound Med. Biol. 2000; 26:1177. [PubMed: 11053753]
33. Lo AH, Kripfgans OD, Carson PL, Rothman ED, Fowlkes JB. IEEE T. Ultrason. Ferr. 2007; 54:933.
34. Barnett SB, Ter Haar GR, Ziskin MC, Rott HD, Duck FA, Maeda K. Ultrasound Med. Biol. 2000; 26:355. [PubMed: 10773365]
35. Castro CI, Briceno JC. Artif. Organs. 2010; 34:622. [PubMed: 20698841]
36. Diaz-Lopez R, Tsapis N, Fattal E. Pharm. Res. 2010; 27:1. [PubMed: 19902338]
37. Mattrey RF. Am. J. Roentgenol. 1989; 152:247. [PubMed: 2643258]

38. Le TD, Weers JG. J. Phys. Chem. 1995; 99:6739.
39. Mezyk SP. J. Phys. Chem. 1995; 99:13970.
40. Borkent BM, Arora M, Ohl CD, De Jong N, Versluis M, Lohse D, MoRch KA, Klaseboer E, Khoo BC. J. Fluid Mech. 2008; 610:157.
41. Raisinghani A, DeMaria AN. Am. J. Card. 2002; 90:3J.

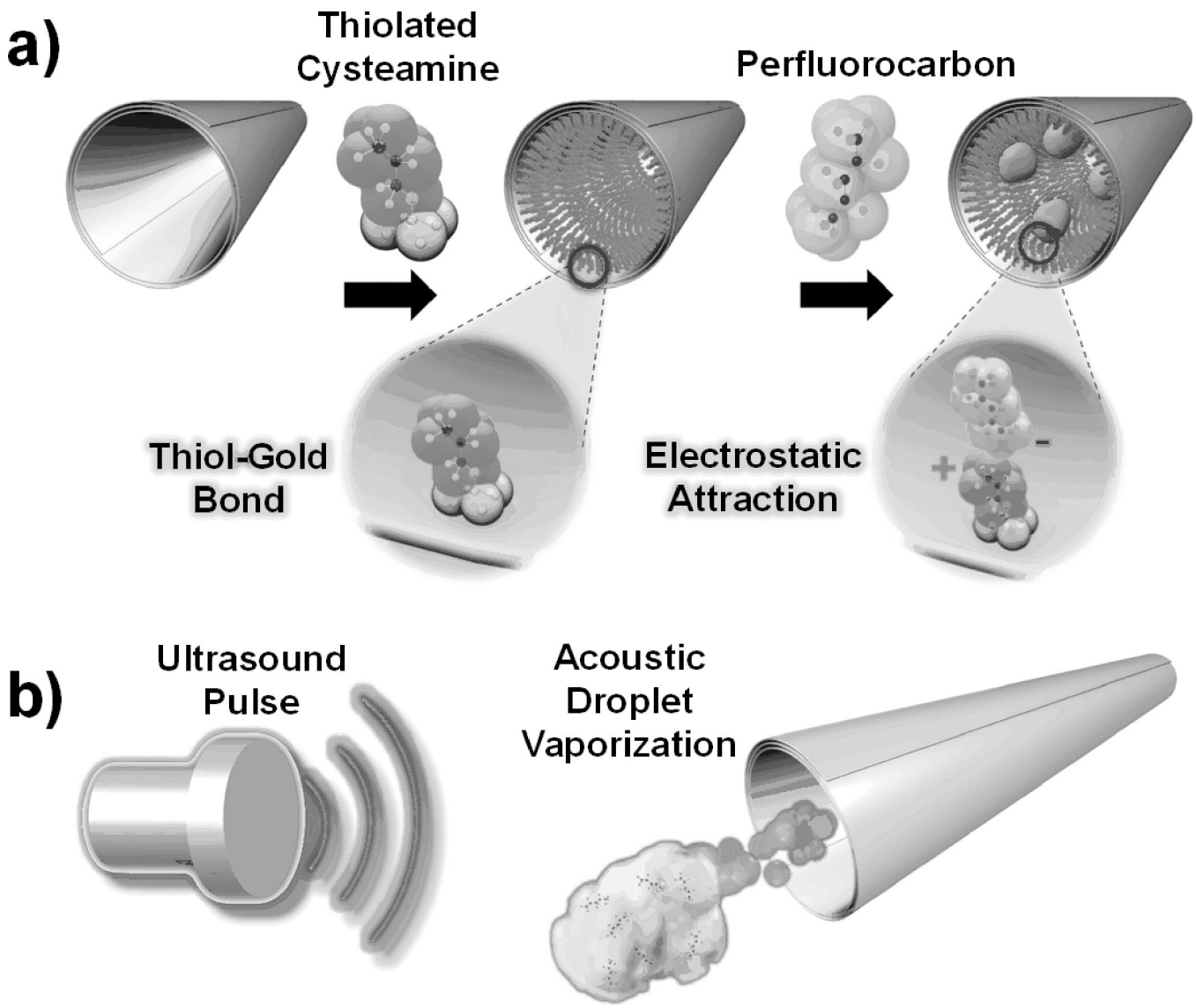

Figure 1.

(a) Preparation of the perfluorocarbon (PFC)-loaded microbullets (MBs): (left) nanofabricated MB, the (middle) conjugation of thiolated cysteamine to the inner Au layer of the MB, (right) electrostatic binding of the anionic PFC emulsion to the cysteamine functionalized surface. Insets show magnified views of (left) cysteamine and (right) cysteamine electrostastically bound to PFC respectively. (b) Schematic portrayal of microbullet propulsion via acoustic droplet vaporization of the bound PFCs triggered by an ultrasound pulse.

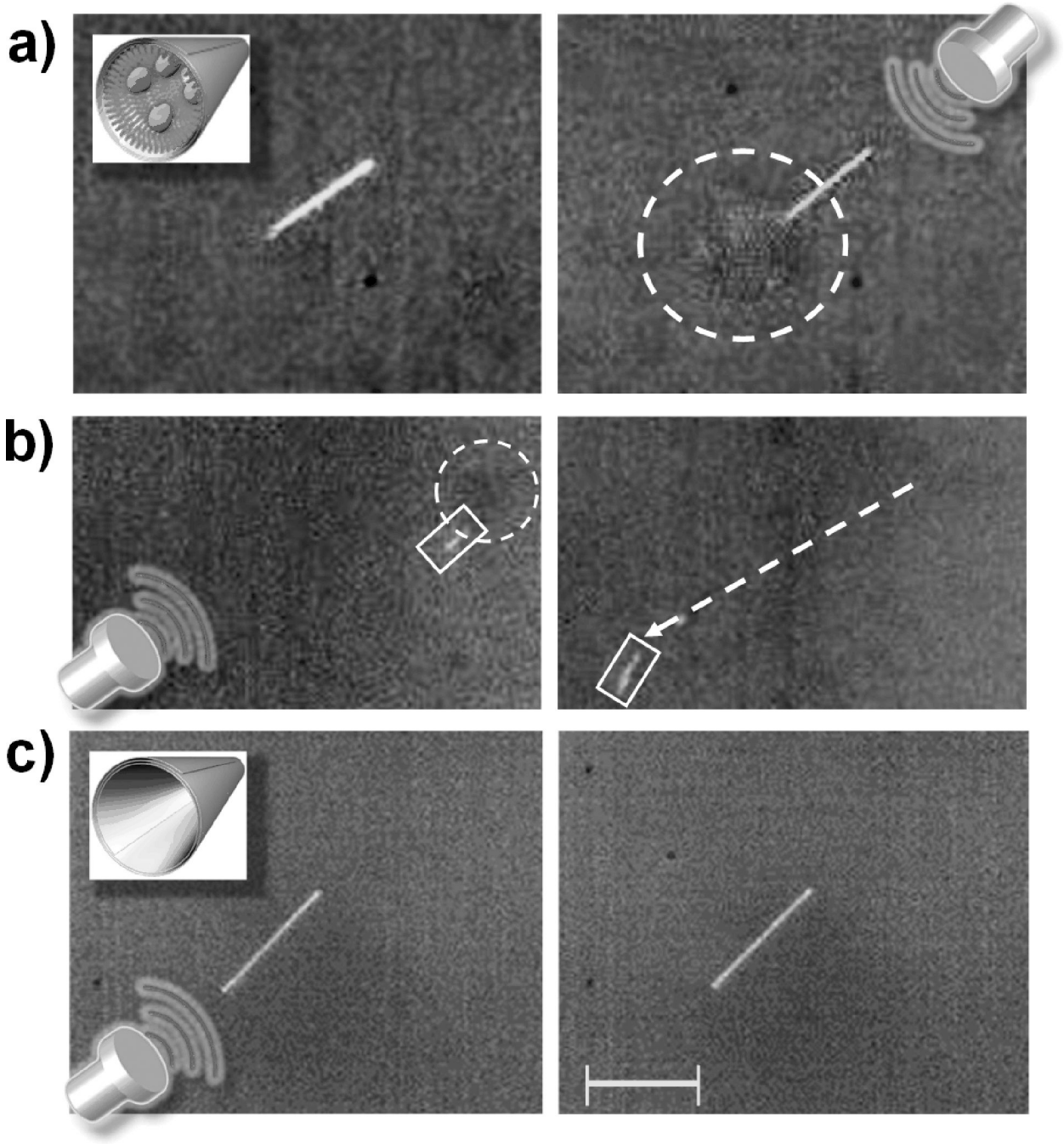

Figure 2.

(a) Still frame images illustrating the formation of a bubble cloud from the tail of perfluorohexane (PFH)-loaded microbullet (MB) upon firing of an ultrasound (US) pulse signal. (b) The trajectory (dotted arrow) of a (right) PFH-loaded microbullet is imaged 55 μs after an (left) US pulse signal. A dotted circle accents the emerging vaporized PFH while boxes highlight the location of the MB. (c) A MB incubated with PFH emulsion but not conjugated with cysteamine displays no emulsion expansion nor movement after a US pulse signal. Inset images show the (a) PFH-loaded MB and the (c) control MB (i.e., without cysteamine) while the US icon represents a US-triggered pulse signal (44 μsec, 1.6 MPa).

Images obtained at a frame rate of 18,000 fps using a 40X objective. Scale bar, 40 μm (a, c) and 120 μm (b).

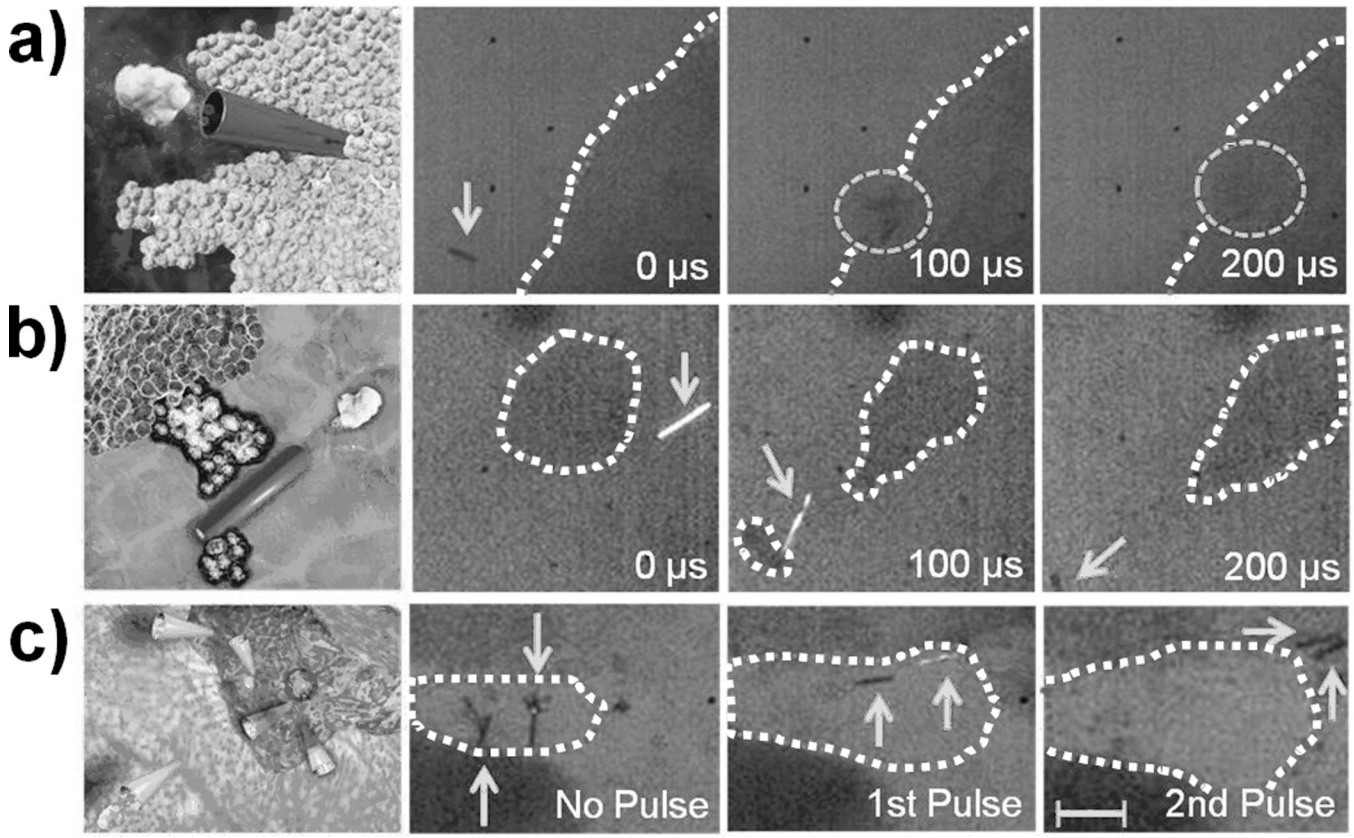

Figure 3.

Computer-aided graphic and corresponding experimental images of PFH-loaded MBs (a) penetrating, (b) cleaving, and (c) expanding a tissue following an US pulse signal, respectively. All images were taken sequentially at a frame rate of 10,000 fps and 10X objective. US pulses of 44 μsec/1.6 MPa were used for (a, b) and short 4.4 μsec/3.8 MPa were used for (c). Dotted circles and solid arrows are used to indicate the MB's position, while curvilinear dotted lines outline the tissue. Scale bar = 100 μm in (a), 40 μm in (b), and 80 μm in (c).